PHILOSOPHICAL TRANSACTIONS A

royalsocietypublishing.org/journal/rsta

Review

Cite this article: Javadi A, Arrieta J, Tuval I, Polin M. 2020 Photo-bioconvection: towards light control of flows in active suspensions. *Phil. Trans. R. Soc. A* **378**: 20190523. http://dx.doi.org/10.1098/rsta.2019.0523

Accepted: 19 June 2020

One contribution of 13 to a theme issue 'Stokes at 200 (part 2)'.

Subject Areas:
biophysics, fluid mechanics

Keywords:
bioconvection, phototaxis, microalgae

Authors for correspondence
A. Javadi
e-mail: arman.javadi@warwick.ac.uk
M. Polin
e-mail: m.polin@warwick.ac.uk

Photo-bioconvection: towards light control of flows in active suspensions

A. Javadi[1], J. Arrieta[3], I. Tuval[3,4] and M. Polin[1,2]

[1]Department of Physics, and [2]Centre for Mechanochemical Cell Biology, University of Warwick, Gibbet Hill Road, Coventry CV4 7AL, UK

[3]Instituto Mediterráneo de Estudios Avanzados, IMEDEA, UIB-CSIC, 07190 Esporles, Spain

[4]Departamento de Física, Universitat de les Illes Balears, 07122 Palma de Mallorca, Spain

JA, 0000-0003-1260-6168; IT, 0000-0002-6629-0851; MP, 0000-0002-0623-3046

The persistent motility of individual constituents in microbial suspensions represents a prime example of the so-called active matter systems. Cells consume energy, exert forces and move, overall releasing the constraints of equilibrium statistical mechanics of passive elements and allowing for complex spatio-temporal patterns to emerge. Moreover, when subject to physico-chemical stimuli their collective behaviour often drives large-scale instabilities of a hydrodynamic nature, with implications for biomixing in natural environments and incipient industrial applications. In turn, our ability to exert external control of these driving stimuli could be used to govern the emerging patterns. Light, being easily manipulable and, at the same time, an important stimulus for a wide variety of microorganisms, is particularly well suited to this end. In this paper, we will discuss the current state, developments and some of the emerging advances in the fundamentals and applications of light-induced bioconvection with a focus on recent experimental realizations and modelling efforts.

This article is part of the theme issue 'Stokes at 200 (part 2)'.

THE ROYAL SOCIETY PUBLISHING

© 2020 The Author(s) Published by the Royal Society. All rights reserved.

1. Introduction

Quiescent suspensions of swimming microorganisms often spontaneously develop large-scale currents, whirling the microbes around in mesmerizingly complex flows [1]. Changing patterns of tight cell-rich downwelling plumes interspersed with large upwells of low cell concentration can be observed in intertidal pools [2], and are a very familiar sight in the laboratory (figure 1). They reveal macroscopically the incessant activity that is present at the microscale, which distinguishes in a fundamental way the behaviour of these so-called active complex fluids [4] from their passive counterparts such as colloidal suspensions. The emergent hydrodynamic instabilities, called bioconvection, are among the oldest reported collective effects in microbial suspensions [1,5–8]. Proposed as potentially important to enhance microbial growth [9,10], the ecological impact of bioconvective flows has been extensively debated [9,11]. Recently, they have been shown to play an important role in promoting growth within stratified lakes [12], where biomixing is able to homogenize chemicals over thicknesses of up to 2 m. Although bioconvection is often a consequence of the natural tendency of microorganisms to swim upwards owing to non-uniform mass distribution within their bodies (bottom-heaviness) [13,14], in many cases it results instead from cells accumulating in response to environmental physico-chemical stimuli. Responses to chemoattractants (chemotaxis) [15] and light (phototaxis) [16–18] have both been observed to cause or alter bioconvection in microbial suspensions. In turn, this raises the question of whether the external control of stimuli could be used to govern large-scale hydrodynamic instabilities in suspensions of swimming microorganisms, thereby harnessing the activity of the suspension to govern its macroscopic transport properties. Control of chemical gradients can be achieved within microfluidic devices [19–22], but advection of the chemical species by the underlying fluid [23–25] makes this a complex strategy for robust control of flows in macroscopic active matter suspensions. Conversely, arbitrary spatio-temporal patterns of light can be engineered easily, and are independent of ensuing flows within the suspension. Although light scattering by cells can be a complicating factor [26], light affords, in principle, an easy route to control microbial motility, by either speed (kinesis) or direction (taxis). This includes naturally phototactic microalgal species [27], some of which are technologically important [28,29], as well as bacteria with a genetically engineered light response [30,31]. Overall, light is a promising tool to determine microbial accumulation [32–34], and through this modify and control macroscopic flows within active suspensions.

Here we will review the current understanding of the interaction between microbial phototaxis and bioconvection (for a recent general review on bioconvection, see [35]). After summarizing the main mechanism leading to bioconvection in §2, in §3 we will discuss the effect of phototactic perturbations to an underlying bioconvective instability. We will then proceed to review recent studies that are pioneering the use of phototaxis to drive—rather than perturb—hydrodynamic instabilities (§4), and the combination of phototaxis and externally imposed shear flows to alter the macroscopic distribution of phototactic cells (§5). We will then conclude in §6.

2. Bioconvection of microbial suspensions: a quick primer

Bioconvection, the macroscopic recirculation that develops spontaneously in concentrated suspensions of microorganisms, was first observed for bottom-heavy microalgae [1]. In these microorganisms, the centre of mass lies behind the hydrodynamic centre of resistance. This is commonly ascribed to inhomogeneities in the mass distribution within the microbial cell body, although shape asymmetries have been proposed to play an important role [36,37]. Indeed, these have been shown to be the dominant cause of bottom-heaviness in the model microalga *Chlamydomonas reinhardtii* [38]. The gap between the centres of mass and hydrodynamic resistance results in a gravitational torque which biases cell motion upwards [39]. This phenomenon, called gravitaxis, accumulates bottom-heavy cells at the upper surface. As cells are usually denser than the surrounding fluid, the accumulation makes the ensuing stratification gravitationally unstable, leading to the development of plumes and convective rolls in a manner similar to

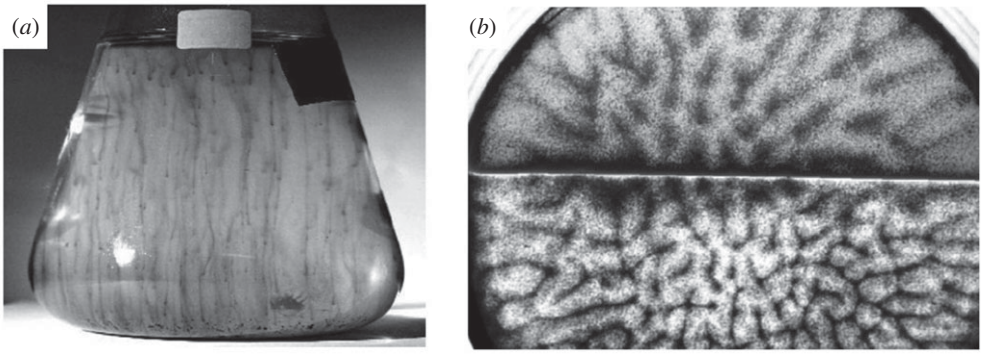

Figure 1. Bioconvective plumes and pattern formation. (*a*) Long vertical gyrotactic plumes in a culture flask. (*b*) Pattern formation in a shallow Petri dish (depth 0.4 cm; width 5 cm; 10^6 cells cm^{-3}); the illumination is white from below, where the lower half is covered with a red filter (660 nm; contrast enhanced). The two regions display different bioconvection patterns: in the top half, white illumination leads cells to swim upwards, with phototaxis supporting gravitaxis and suppressing gyrotaxis, initiating an overturning instability with broad downwelling structures; in the bottom half, cells do not respond to the red illumination and form finely focused gyrotactic plumes. Adapted from [3].

Rayleigh–Bénard convection. Sinking bioconvective plumes are then reinforced by gyrotaxis, the tendency of bottom-heavy cells to move towards downwelling regions resulting from the balance between gravitational and hydrodynamic torques originally observed in pipe flow by Kessler [39]. A continuum model for gyrotactic bioconvection of a dilute suspension of swimming microorganisms was first studied by Pedley *et al*. [40] and then by Pedley & Kessler [14,41] (figure 2*a*). Here, the suspension of algal cells is modelled as a continuum of identical prolate ellipsoids of volume v and density ρ_c that swim with a constant speed V_s along a direction $\boldsymbol{p}$ and do not interact directly with each other. The swimming direction is determined by a combination of environmental torques acting on the cell and the randomness inherent in microbial swimming, and is therefore described locally by a probability distribution $f(\boldsymbol{p})$. This is taken to satisfy a quasi-steady Fokker–Planck (FP) equation, balancing advection by currents in $\boldsymbol{p}$—due to gravitational and hydrodynamic torques—with an effective angular diffusion of diffusivity D_R due to cell swimming. If the concentration of cells at position $\boldsymbol{x}$ and time t is $n(\boldsymbol{x}, t)$, and $\boldsymbol{u}(\boldsymbol{x}, t)$ and p represent the velocity and pressure of the underlying fluid, respectively, the governing equations for the system are [41]

$$\nabla \cdot \boldsymbol{u} = 0, \tag{2.1}$$

$$\rho\left(\frac{\partial \boldsymbol{u}}{\partial t} + \boldsymbol{u} \cdot \nabla \boldsymbol{u}\right) = -\nabla p + \nabla \cdot (2\mu \boldsymbol{E} + \boldsymbol{\Sigma}) + nv\Delta\rho \boldsymbol{g}, \tag{2.2}$$

$$\frac{\partial n}{\partial t} + \nabla \cdot (n(\boldsymbol{u} + \boldsymbol{V})) = \nabla \cdot (\mathbf{D} \cdot \nabla n), \tag{2.3}$$

$$\nabla_{\boldsymbol{p}} \cdot (f\dot{\boldsymbol{p}}) = D_R \nabla_{\boldsymbol{p}}^2 f \tag{2.4}$$

and

$$\dot{\boldsymbol{p}} = (\mathbf{I} - \boldsymbol{pp}) \cdot \boldsymbol{\Omega} \cdot \boldsymbol{p} + \Lambda\left(\mathbf{I} - \boldsymbol{pp}\right) \cdot \boldsymbol{E} \cdot \boldsymbol{p} + \frac{1}{B}(\mathbf{I} - \boldsymbol{pp}) \cdot \boldsymbol{k}. \tag{2.5}$$

Here we recognize the Navier–Stokes equations for a fluid of density ρ and dynamic viscosity μ. Mass conservation (equation (2.1)) enforces fluid incompressibility, and momentum balance (equation (2.2)) is governed by the rate of strain tensor, $\boldsymbol{E} = (\nabla \boldsymbol{u} + \nabla \boldsymbol{u}^{\mathrm{T}})/2$, the buoyancy forces caused by the excess cell density ($\Delta\rho = \rho_c - \rho$) considered within the Boussinesq approximation (with $\boldsymbol{g}$ being the gravitational acceleration), and the excess deviatoric stress $\boldsymbol{\Sigma}$, which will be discussed in detail below. Local cell conservation, (equation (2.3)) depends on the cells' effective diffusion tensor $\mathbf{D}$, which is non-isotropic for gravitactic species [42], and on advection by both the

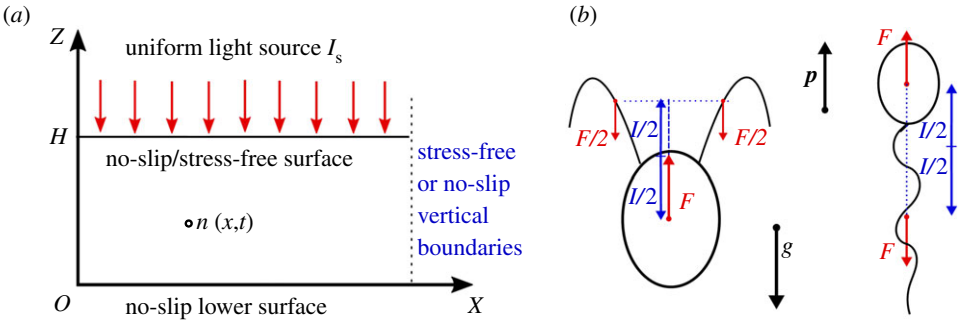

Figure 2. Standard setting for photo-bioconvection. (*a*) The cell suspension, of instantaneous local cell density $n(\boldsymbol{x}, t)$, is contained within a horizontal chamber of thickness H. The bottom surface is no-slip, while the top surface can be either no-slip or no-stress. The suspension is subjected to a uniform vertical illumination of intensity I_s. (*b*) Typical structures of the main types of swimming microorganisms. Left: a biflagellate microalga (puller-like). Right: a bacterium (pusher-like). Both swim along the direction $\boldsymbol{p}$ and are subjected to gravity, with gravitational acceleration $\boldsymbol{g}$. (Online version in colour.)

local fluid flow and swimming speed $\boldsymbol{V}$. The cells' gravitational sedimentation has been neglected in this formulation, but its effect was later investigated by Pedley [13,43]. The average swimming velocity $\boldsymbol{V} = V_s\langle \boldsymbol{p}\rangle$, where $\langle \boldsymbol{p}\rangle$ is the local average swimming direction,

$$\langle \boldsymbol{p}\rangle = \int_{S^2} \boldsymbol{p} f(\boldsymbol{p})\, \mathrm{d}^2\boldsymbol{p}. \tag{2.6}$$

Note that, although $\boldsymbol{p}$ is a unit vector, the magnitude of $\langle \boldsymbol{p}\rangle$ can range from 0 (completely random swimming) to 1 (all cells swimming along the same direction). Changes in the local distribution of cell orientation and the effect of local environmental torques on the swimming direction $\boldsymbol{p}$ are modelled by equations (2.4) and (2.5). Here, the distribution function $f(\boldsymbol{p})$ is the solution of a quasi-steady advection–diffusion equation on the unit sphere S^2 with effective rotational diffusivity D_R. This approach slaves $f(\boldsymbol{p})$ to the instantaneous local orientational currents $\dot{\boldsymbol{p}}$, a valid assumption if temporal changes in the local flow structure are slow compared with the intrinsic equilibration time scale of the local distribution of cell orientations. Equation (2.5), in turn, describes how a cell's swimming direction $\boldsymbol{p}$ changes as a result of viscous and gravitational torques. The former is a combination of uniform rotation (from the local vorticity $\boldsymbol{\Omega} = (\nabla \boldsymbol{u} - \nabla \boldsymbol{u}^{\mathrm{T}})/2$) and alignment along the principal extensional direction (from the rate of strain tensor $\boldsymbol{E}$). The relative importance of these terms depends on the shape parameter Λ, which measures the cell's eccentricity [44]. It is zero for a spherical organism, and tends to unity for rod-like swimmers [44]. This is responsible for the famous Jeffery orbits of elongated ellipsoids in shear flow [45]. The last term on the right-hand side, instead, is the gravitational torque due to bottom-heaviness, with the gravitational reorientation time scale B determined by the balance between the maximal gravitational torque and the viscous resistance to rotation [46],

$$B = \frac{\mu \alpha_\perp}{\rho_c g h}. \tag{2.7}$$

Here $\alpha_\perp$ is the resistance coefficient for the cell's rotation about an axis perpendicular to $\boldsymbol{p}$ and h is the centre-of-mass offset of the cell. Note that the physical implication of any term of the form $(\mathbf{I} - \boldsymbol{pp}) \cdot \boldsymbol{e}$ on the right-hand side of equation (2.5) is to rotate and align $\boldsymbol{p}$ along $\boldsymbol{e}$.

We have not yet discussed the term $\boldsymbol{\Sigma}$, added to the stress tensor in equation (2.2). This accounts for the stress contribution of the cells to the ambient fluid flow, and is the sum of two terms, $\boldsymbol{\Sigma} = \boldsymbol{\Sigma}_p + \boldsymbol{\Sigma}_s$. The former is a passive term due to the disturbance flow field caused by the rigid cell bodies ($\boldsymbol{\Sigma}_p$), which follows the expression derived by Batchelor for a suspension of identical rigid passive particles [47]. The latter is an active stress term from cell motility which comes from the stresslet contribution to the forces exerted by a swimming cell on the surrounding

fluid. If the magnitude of the drag force from the body on the liquid is F, and this is countered—on average—by an equal and opposite thrust from the motile appendages at a distance l from the hydrodynamic centre of the body, the $\boldsymbol{\Sigma}_s$ is given by [46]

$$\boldsymbol{\Sigma}_s = \pm nFl\left(\langle \boldsymbol{pp}\rangle - \frac{1}{3}\mathbf{I}\right), \tag{2.8}$$

where n—as above—is the local cell concentration, and the sign choice depends on whether the microswimmers are of puller (+) or pusher (−) type (figure 2*b*). Pedley and Kessler [41,46] showed that this is by far the dominant contribution, and therefore only the active stress contributions ($\boldsymbol{\Sigma}_s$) are taken into account in equation (2.2). Taking $\boldsymbol{\Sigma} \simeq \boldsymbol{\Sigma}_s$ and using equation (2.8) gives a good approximation of the effects of swimmers on the flow in dilute suspensions (with typical cell densities of the order of 10^6 cells cm^{-3}) and has been used extensively throughout the literature on collective motion. However, it can also be neglected in many situations with pre-existing background flows that have characteristic viscous stresses much larger than $\|\boldsymbol{\Sigma}_s\|$.

Besides contributing to the fluid's stress tensor, cell swimming leads also to an effective diffusivity tensor $\mathbf{D}$. For the constant swimming speed V_s assumed here, it can be derived from the Green–Kubo relations as [41,48,49]

$$\mathbf{D} = \int_0^\infty \left\langle \boldsymbol{V}_r(t)\boldsymbol{V}_r(t-t')\right\rangle \mathrm{d}t'; \quad \boldsymbol{V}_r \equiv V_s(\boldsymbol{p} - \langle \boldsymbol{p}\rangle), \tag{2.9}$$

which, under the assumption of a constant correlation time τ, reduces to [13]

$$\mathbf{D} = V_s^2\tau\left\langle(\boldsymbol{p} - \langle \boldsymbol{p}\rangle)(\boldsymbol{p} - \langle \boldsymbol{p}\rangle)\right\rangle. \tag{2.10}$$

Typical values of τ range between 1 s and 5 s. These expressions assume that the background fluid shear does not influence fluctuations and persistence in cell orientation. The validity of this approximation in a real system is uncertain, especially for large shear rates. As a result, Hill & Bees (for spherical swimmers [42]) and Manela & Frankel (for axisymmetric swimmers [50]) have used instead a generalized Taylor dispersion (GTD) theory to formulate the diffusivity of a suspension of gyrotactic micro-swimmers. For sufficiently low shear rates, the difference between the two approaches is not significant, and the previous—simpler—approach to $\mathbf{D}$ can be used for example to study the initial development of bioconvection from a quiescent background fluid. The stability of the suspension is generally described in terms of a Rayleigh number for active particles $R = \bar{n}gv\Delta\rho H^3/(\mu D)$, which depends on the ratio between buoyancy and viscous forces and the ratio between diffusion of momentum within the fluid and active diffusion. Here $\bar{n}$ is the average cell concentration and H is the container thickness. Through linear stability analysis of equations (2.1)–(2.5), it is possible to predict the onset of the instability, in terms of a critical Rayleigh number, and the most unstable wavelength, usually called the bioconvective wavelength, which should then correspond to the characteristic separation between plumes observed experimentally (figure 3*b*,*c*) [35,51].

The approach that we have briefly outlined offers in general a good qualitative description of the experimental observations of bioconvection. Quantitatively, however, the agreement is often less good. For shallow suspensions, for example, theoretical predictions overestimate the observed wavelengths (observed: approx. $1-3$ mm versus predicted: approx. 4–7 mm [40,54,55]), although better agreement can be obtained by leaving constitutive microbial parameters ($B, \tau, V_s \ldots$) as variables to be fitted [56]. Pedley and Kessler have also suggested that the actual nonlinear nature of the instability might be a cause of the observed discrepancy between the characteristic wavelength for bioconvection observed experimentally and the one predicted from linear stability analysis [41]. Much of the quantitative uncertainty must also come from our limited knowledge of the swimming behaviour of the microorganisms within the suspension, and possibly of their ability to sense and react to mechanical stresses [57,58]. Finally, bioconvection experiments show clearly three-dimensional patterns. Therefore, in principle, the full three-dimensional problem should be solved for a true quantitative comparison between theory and experiments. Recent three-dimensional simulations are starting to address this issue [59–61], and

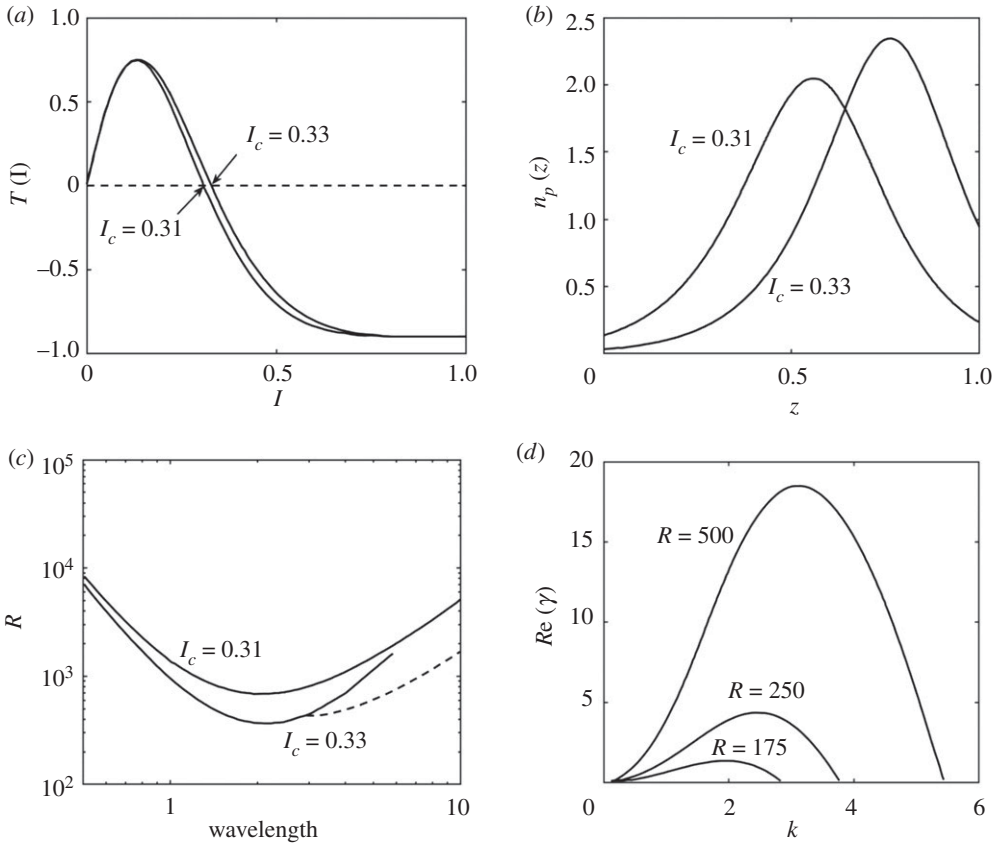

Figure 3. Penetrative bioconvection. (*a*) Taxis functions corresponding to different values of I_c (non-dimensionalized), and (*b*) corresponding equilibrium profiles of cell concentration (for $I_s = 0.5$). In this example, despite being close in value, the critical light intensities are well separated in space owing to the slow decay of the intensity profile ($\alpha\bar{n}H = 1$). (*c*) Neutral curves separating stable perturbations (below) from unstable ones (above). (*d*) The perturbations' growth rate depends strongly on the Rayleigh number. Adapted from [52,53].

in particular Ghorai *et al.* [61] found characteristic wavelengths that were in good agreement with previous experiments [55], provided that the diffusion due to randomness in cell swimming behaviour is small.

3. Phototactic modifications to standard bioconvection

The general framework presented in §2 served as a starting point for the first studies on the effects on bioconvection of phototaxis, the ability of some microbial species (e.g. green microalgae [62] and dinoflagellates [63]) to swim towards a light source (positive phototaxis) or away from it (negative phototaxis). The light needs to be within the range of wavelengths which the light-sensitive organelles are sensitive to (approx. 420–500 nm for *Chlamydomonas* [64]), which overlaps with—but does not necessarily exactly correspond to—the photosynthetically active range [65]. The pioneering continuum studies of photo-bioconvection [66] considered purely phototactic cell suspensions that are exposed to uniform illumination from above or below (figure 2*a*). Swimming cells are still assumed to be slightly heavier than the ambient fluid, but gyrotaxis and gravitaxis are neglected and the upswimming is exclusively due to phototaxis. The swimming velocity, however, depends on the intensity of light I, with positive phototaxis for light intensity below a critical value I_c ($I < I_c$), and negative phototaxis otherwise ($I > I_c$). This captures the fact that

phototactic organisms move away from intense light to avoid photodamage [27], and results in a tendency to accumulate cells where $I \approx I_c$. The swimming velocity in equation (2.3) is then

$$\boldsymbol{V} = V_s T(I)\boldsymbol{k}, \quad \text{where } T(I) \begin{cases} \geq 0, & I \leq I_c, \\ < 0, & I > I_c. \end{cases} \tag{3.1}$$

Here $\boldsymbol{k}$ is the vertical unit vector and $T(I)$ is the phenomenological taxis function with values between -1 and $+1$ (figure 3*a*). The shape of the taxis function is, in principle, species dependent, and is usually constructed based on the simplification of controlled experimental observations [52]. At the same time, the diffusion tensor is assumed to be constant and isotropic. This non-monotonic response to light is coupled to changes in light intensity owing to the absorption and scattering of light by cells, or 'shading'. This phenomenon is particularly important for dense cell suspensions such as those that can be achieved in the laboratory or within bioreactors. For thick but sufficiently dilute suspensions, the local scattering of light by the cells is weak and the light intensity $I(\boldsymbol{x}, t)$ is simply given by the Beer–Lambert law [53],

$$I(\boldsymbol{x}, t) = I_s \exp\left(-\alpha \int_z^H n(\boldsymbol{x}, t)\, \mathrm{d}z\right), \tag{3.2}$$

where I_s is the uniform light intensity at the upper surface of the suspension ($z = H$) and α is the absorption coefficient. The rigid bottom with a no-slip boundary condition is located at $z = 0$. Light intensity is therefore a monotonically decreasing function of depth (z). If I_c lie between the maximum and minimum intensities across the suspension, a sublayer of cell concentration is formed in the interior of the chamber (figure 3*b*). The region above this sublayer is gravitationally stable and it is resting on a gravitationally unstable region below. The bottom layer can then develop circulating flows that penetrate the stable layer, resulting in bulk motion throughout the suspension [67]. This phenomenon is called penetrative bioconvection. Linear instability analysis showed that, within this model, the onset of the instability and the length scales of the ensuing patterns depend on the average cell concentration, the position at which $I = I_c$ for a uniform suspension, and the depths of the gravitationally stable and unstable layers (figure 3*b*,*c*). Depending on the values of the parameters, this model can develop two different types of large-scale flows, either steady or periodic. The former is the usual type of bioconvective flow. The latter corresponds to oscillating flow and concentration fields that occur when upswimming due to phototaxis is dominant over convective downwelling. Panda *et al.* [68] extended Ghorai and Hill's work to show that these instabilities are opposed by the presence of rigid side walls, which enhance stability for some parameter regimes.

The models above usually rest on two major assumptions: they neglect light scattering from the cells, implying that each cell only receives light vertically from the uniformly illuminating source; and they neglect bottom-heaviness and therefore gyrotaxis. Let us consider these assumptions individually. If light scattering from cells is important, then each cell will have to respond to multiple stimuli besides the main one from the illuminating source. This was first discussed by Ghorai *et al.* [53] by introducing a radiative transfer equation for the direction-dependent light intensity and a scattering probability that determines the likelihood for light to be scattered by a given amount. Both isotropic and anisotropic scattering probabilities were studied [26,69]. The inclusion of scattering complicates the model significantly and makes it a formidable task to find the intensity profile $I(\boldsymbol{x})$, which needs to be solved for together with the fluid flow and cell concentration. Linear stability analysis [53] and two-dimensional numerical solutions [69] reveal that, for purely scattering suspensions, the intensity $I(\boldsymbol{x})$ may not vary monotonically with depth. A suspension can therefore exhibit more than one location where $I = I_c$, leading to an altered base state from the single sublayer discussed earlier. Besides this difference, light scattering from cells does not seem to introduce any qualitatively new instabilities within the suspension [53]. However, it should be stressed that these results hinge on a specific simple model of phototaxis. Light scattering by cells generates light fields with multiple sources, and our knowledge of

phototaxis in this situation is currently poor. Although it has been investigated for gliding motility in cyanobacteria [70], it is not a well-understood process for swimming cells.

Thus far, we have only considered models for pure phototaxis, where upswimming was just a consequence of cells' motion towards light. Many microorganisms, however, are also gravitactic and gyrotactic and should, in principle, be taken into account to describe the suspension's dynamics. The first model of this kind, which modified Pedley and Kessler's model (§2) to account for phototaxis, was proposed by Williams & Bees [17]. They considered three different models to incorporate the effects of phototaxis: a photokinesis model where a cell's swimming speed is a function of light intensity (A); a coupled photo-gyrotactic model where light controls the position of a cell's centre of mass, and therefore its bottom-heaviness (B); and an extra 'phototactic torque' in equation (2.5) to reorient cells along gradients of light intensity (C). We note that it has recently been demonstrated that some microbial species can modify their fore–aft mass asymmetry in response to mechanical stimuli [71], and it would not be far fetched to expect that, in some cases, this might also be true for light stimuli. Overall, the models proposed by Williams and Bees are an excellent starting point to investigate the coupling between photo- and gyrotaxis. They lead to changes in equations (2.3) and (2.5), which become

$$\frac{\partial n}{\partial t} + \nabla \cdot n\left(\boldsymbol{u} + \underbrace{V_s\left(1 - \frac{I}{I_c}\right)}_{\text{(A)}}\langle \boldsymbol{p}\rangle\right) = \nabla \cdot (\boldsymbol{D} \cdot \nabla n) \tag{3.3}$$

and

$$\dot{\boldsymbol{p}} = \underbrace{\frac{1}{B(I)}}_{\text{(B)}}(\boldsymbol{I} - \boldsymbol{pp}) \cdot \underbrace{\boldsymbol{k}(I)}_{\text{(C)}} + (\boldsymbol{I} - \boldsymbol{pp}) \cdot (\boldsymbol{\Omega} \cdot \boldsymbol{p} + \Lambda \boldsymbol{E} \cdot \boldsymbol{p}), \tag{3.4}$$

where V_s is now the swimming speed in the absence of any illumination and I_c is the critical intensity from equation (3.1). Model (A) includes an intensity-dependent speed in equation (3.3) that encodes both a photokinetic effect (i.e. swimming speed that depends on light intensity) and the ability of the cells to reverse their swimming direction in regions where $I > I_c$. The other two models, instead, modify the equation for the cell orientation (equation (2.5)), and therefore the value of $\langle \boldsymbol{p}\rangle$. The new equation (equation (3.4)) includes either an intensity-dependent gravitational reorientation time scale $B(I)$ (model B) or an intensity-dependent preferred cell orientation $\boldsymbol{k}(I)$ (model C). The former is an *ad hoc* manifestation of the cell's ability to change its centre-of-mass offset as a function of I, which is taken to follow

$$B(I) = \frac{\mu \alpha_\perp}{\rho_c g h_0 (1 - I/I_c)}, \tag{3.5}$$

where h_0 is the centre-of-mass offset in the dark (see also equation (2.7)). This assumes that bottom-heavy cells become top-heavy for $I > I_c$. The latter is the effect of the phototactic torque. The preferred cell orientation $\boldsymbol{k}(I)$ is obtained by balancing the gravitational torque $\boldsymbol{L}_g = (\rho_c v g h_0)\boldsymbol{p} \times \boldsymbol{k}$ and the phototactic torque

$$\boldsymbol{L}_p = -\frac{4 f_m}{I_c^2} I(I - I_c)\boldsymbol{p} \times (\beta_1 \boldsymbol{\pi} + \beta_2 \nabla I). \tag{3.6}$$

Here f_m is a parameter defining the overall strength of the phototactic torque, while β_1 and β_2 quantify the cell's phototactic response to light incident from an arbitrary direction $\boldsymbol{\pi}$ and to local gradients in the light intensity. Then $\boldsymbol{k}(I)$ is simply given by

$$\boldsymbol{k}(I) = \boldsymbol{k} + \frac{4 f_m}{m g h_0}\left(\frac{I}{I_c}\right)\left(\frac{I}{I_c} - 1\right)(\beta_1 \boldsymbol{\pi} + \beta_2 \nabla I). \tag{3.7}$$

Williams and Bees studied these three models separately, with two cases considered for model C: $(\beta_1, \beta_2) = (1, 0)$ (C I) or $(0, 1)$ (C II). In general, phototaxis will affect the probability distribution $f(\boldsymbol{p})$ (equation (2.4)), and through this the quantities $\langle \boldsymbol{p}\rangle$ (equation (2.6)) and $\boldsymbol{D}$ (equation (2.9)) in a non-trivial way [17]. The coupled photo-gyrotaxis models are able to predict both steady and

oscillating flow patterns. Interestingly models A, B and C I produce very similar results, when illuminated from above, which also agree qualitatively with experiments carried out by Williams & Bees [3]. The basis for this comparison with experiments, however, was deemed questionable for several reasons. Firstly, the experimental methods did not allow for the theoretical base state to be reached before instabilities appeared; secondly, there was a lack of reliable direct estimates of the critical intensity I_c for the suspension; and finally it was unclear whether the wavelengths being measured in the experiment corresponded to the critical state obtained using the theory. Nevertheless, the qualitative agreement observed between models and experiment is promising. At the same time, model C II differs significantly from the others owing to the existence of non-hydrodynamic instabilities. In this case, phototactic torques due to ∇I lead to horizontal modulations of the cell concentration profile, with equally spaced clusters of cells just above the depth at which $I = I_c$ for the (unstable) base state. This modulation should happen without generating a background fluid flow. Finally, we note that a formal extension of GTD to a suspension of phototactic microorganisms, in the spirit of the work of Hill & Bees [42], Manela & Frankel (for gyrotaxis) [50] and Bearon *et al.* (for chemotaxis) [72–74], has not been attempted yet. It will be interesting to see how GTD alters the stability dynamics of phototactic suspensions.

4. Bioconvection driven by phototaxis

A recent experimental endeavour is to use light as the main factor leading to bioconvection. In these studies, no bioconvection patterns are observed in the absence of light. Convective instabilities only appear in the presence of specific illumination patterns used to generate the cell-density inhomogeneity that drives bioconvection.

The first instabilities of this type were investigated in suspensions of the microalga *Euglena gracilis* [16,75]. Initially homogeneous cultures filled the gap within a 2-mm-thick horizontal Hele–Shaw cell, and were then exposed to strong uniform illumination from the bottom to induce negative phototaxis. Within a few minutes, cells accumulated in randomly distributed high-density clusters [16], which then gathered towards the centre of the chamber. These localized patterns disappeared in the absence of light. The number of clusters and the mean separation between neighbouring clusters can be used to characterize the dynamics of the system as a function of the depth of the chamber and average cell concentration. Both quantities showed ageing, with the former increasing and the latter decreasing as a function of time. An effective model based on transition probabilities between cell layers was able to recapitulate the qualitative dynamics of cell concentration observed experimentally, including the process of pattern formation, cell circulation around a cluster and the dependence of the number of clusters and their distance to nearest neighbours on the depth and cell density. This agreement provided support for the hypothesis that pattern formation is a consequence of cell motion transversal to the direction of incoming light, possibly as a result of phototaxis to light scattered by the microorganisms themselves. Although this model lacks a connection to the underlying hydrodynamics of the suspension, it is still a first step towards understanding the emergence of photo-bioconvective patterns. A later study of localized photo-bioconvection patterns in the same system [76] showed that the emergence of these high-density cell clusters, or 'bioconvection units', was dependent on the spatial distribution of the cells before light exposure. Below a critical cell concentration, no bioconvection units were observed for a uniform initial distribution, whereas a single cluster formed for sufficiently spatially heterogeneous suspensions. This observation suggests that the system is multi-stable, possibly as a result of the topology of the containing chamber.

In an interesting study by Dervaux *et al.* [77], intriguing bioconvective instabilities were observed instead when a thin suspension of the model unicellular green algae *C. reinhardtii* was placed in a Petri dish and illuminated from above by a localized circular laser beam. For intensities within the range of positive phototaxis, the cells accumulated beneath the light beam, and radially symmetric convective flows developed as a result of light-induced

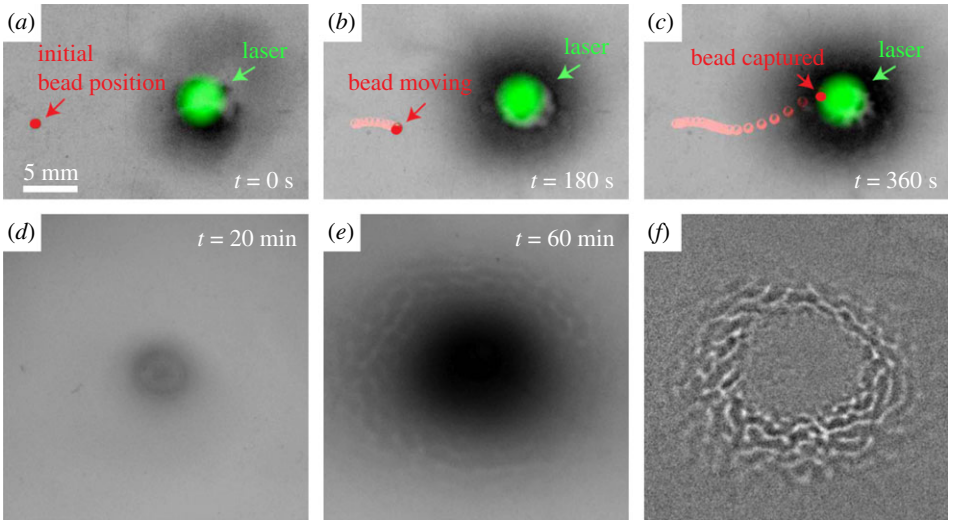

Figure 4. Photo-bioconvection induced by localized laser illumination in [77]. (*a–c*) An 800-µm-diameter floating glass bead is transported by the flow field generated by the concentrated cells. (*d–f*) Time evolution of phototactic cell accumulation at the bottom of the container and formation of radial waves of concentration. Adapted from [77]. (Online version in colour.)

collective motion. Although the time scale for the establishment of this instability was long (approx. 1 h), the ensuing convergent flows on the surface could be used to collect a floating cargo (here a 800 µm glass bead) and trap it just above the laser spot (figure 4*a–c*). Above a critical Rayleigh number, corresponding to high cell density and layer depth, a novel instability in the form of travelling concentration waves was discovered (figure 4*d–f*). Its development was successfully described through a model for cell reorientation that included turning due to the fluid's vorticity, and a phototactic reorientation similar to the first term in equation (3.4), but with $\boldsymbol{k}$ replaced by the direction of ∇I from the laser. The effective time scale for phototactic turning, equivalent to $B(I)$ in equation (3.4), was left as a fitting parameter. Best fits were obtained for a time scale $\simeq 1.2$ s, significantly faster than the gyrotactic reorientation time scale (approx. 3–6 s for *Chlamydomonas augustae*, a species known to be strongly gyrotactic [3]). This work is the first experimental validation of the phototactic torque model in a simplified case.

More recently, Arrieta *et al.* [18] reported a new example of bioconvection driven by phototaxis, which develops quickly (approx. 30 s) and can be easily reconfigured. In this case, a suspension of *C. reinhardtii* is loaded within a thin and wide square chamber held vertically, a configuration notably distinct from similar studies in bioconvection, where the widest sides of the chamber are horizontal. Localized illumination was provided by a 200-µm-diameter horizontal optical fibre. With no light from the fibre, cells were uniformly distributed within the suspension. However, as the light was switched on, the algae accumulated phototactically around the fibre, leading to a gravitational instability and the formation of a single localized sinking bioconvective plume. The system was described with a purely phototactic model of two-dimensional bioconvection, based on equations (2.1)–(2.3), with no slip at the boundary and no cell flux through the boundary. Following previous studies [34], the phototactic velocity was taken to be proportional to the gradient in light intensity. The proportionality factor depends on the phototactic sensitivity parameter, β, previously shown to exhibit an interesting adaptation possibly as a result of the photosynthetic activity of the cells [34]. Despite neglecting gyrotaxis and gravitaxis, as well as cell–cell interactions reinforcing alignment at high concentrations [78], the model showed excellent agreement with experimental observations and was able to capture the structure of the bioconvective flow of cells (figure 5). It also predicted that for average cell densities below

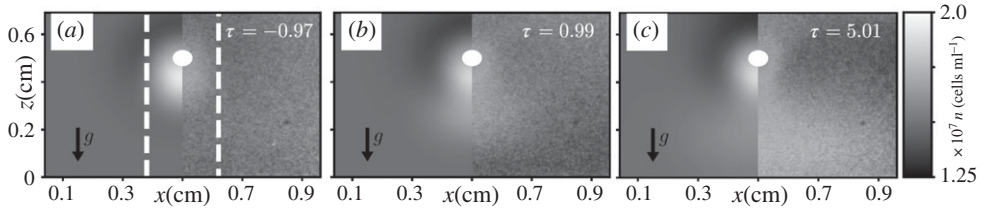

Figure 5. (*a–c*) Dynamics of plume formation in localized photo-bioconvection. Cells accumulate around the optical fibre (white disc) and form a single bioconvective plume as the reduced time τ progresses. Panels show the cell density (n) from the continuum model (left side) and the experiments. Plume formation takes approx. 30 s. Adapted from [18].

a critical value, n_c (approx. 10^7 cells/cm^3 for $\beta = 0.14$), phototactic accumulation around the fibre would not lead to the development of a plume. We note, however, that the background fluid has a global recirculation even when the plume does not form, as a result of the excess concentration of phototactic cells around the optical fibre. The existence of this bifurcation was confirmed experimentally, and the critical cell density observed was in good quantitative agreement with the one predicted by the model. Overall, the model predicted a bifurcation boundary compatible with the simple relation $\beta n_c = \text{const}$. Leveraging the speed at which plumes form in this system, the authors then provided a proof of principle that photo-bioconvection can be used to mix the suspension. This was achieved here by alternately blinking a pair of optical fibres to create two sets of convective flows with crossing streamlines.

5. Photo-focusing

Light can also be used together with externally imposed flows to control the motion of phototactic cells through a mechanism based on balance between hydrodynamic and phototactic torques, analogous to gyrotaxis. This has been proposed to play a role in the cell accumulation observed by Dervaux *et al.* [77] and can be employed to accumulate cells in specific regions by imposing background flows externally. This type of cell accumulation, called photo-focusing, has been investigated in a number of recent studies [33,79–81]. The first direct proof of photo-focusing used a suspension of *C. reinhardtii* flowed through a long square capillary of side 1 mm [79]. The cells' distribution across the channel, which was uniform without light stimuli, could be modulated dramatically by turning on a light source oriented along the length of the channel. When cells tried to phototax downstream they self-focused along the axis of the channel, whereas for upstream phototaxis cells accumulated at the boundaries (figure 6). An initial model for photo-focusing used a deterministic description of microbial swimming within a Poiseuille flow [82], modified by an effective phototactic torque on the cell, and provided a good qualitative description of the phenomenon, including the existence of a threshold fluid vorticity beyond which the suspension does not self-focus. The same system was later studied numerically for a whole suspension of interacting microswimmers [80], where phototaxis was modelled by the *ad hoc* reorientation of each swimmer along the light direction approximately every 1 s. The simulations reproduced the formation of a self-focusing jet for sufficiently low vorticities and predicted the further fragmentation of these jets into clusters. The latter instability, due to hydrodynamic interactions between the puller microorganisms within the model, has yet to be observed experimentally in photo-focused jets, although it bears a striking resemblance to instabilities that develop in gyrotactically focused cells [83]. More recently, the same run-and-tumble-like dynamics was studied in a two-dimensional model of photo-focusing for dilute suspensions, and was shown to reproduce well the experimental data for the scaling of the width of the focusing region and the establishment length as a function of the flow velocity [33]. The agreement between model and experiments provides support for the assumption of an active resistance by the cells to shear-induced turning [57], which was included here as a scaling of the local fluid vorticity by a factor $\eta < 1$. Best fits were obtained for $\eta = 0.25$. Although the details of the phototaxis model used here

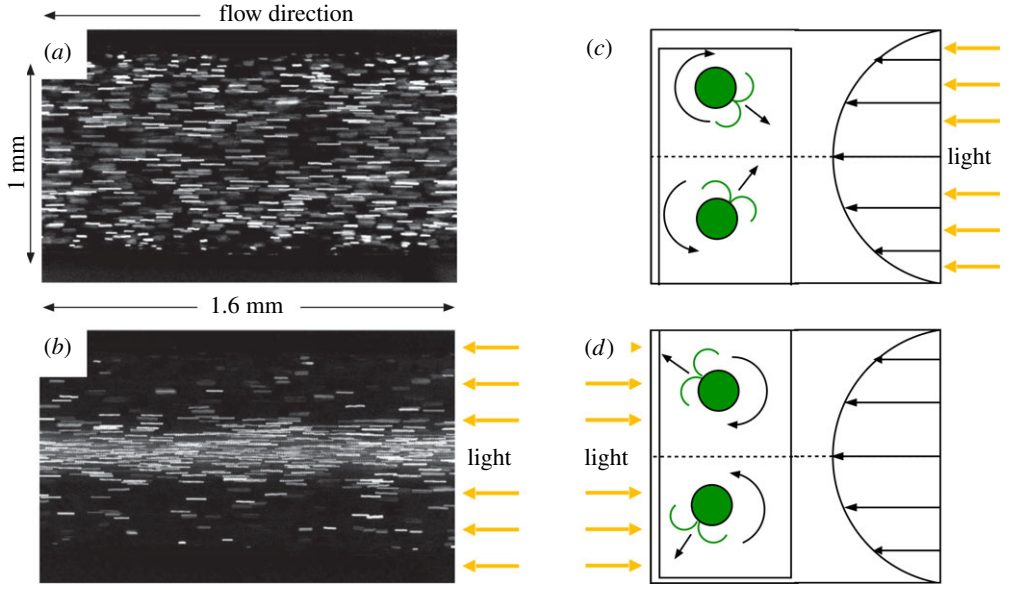

Figure 6. Photo-focusing. Individual trajectories of *C. reinhardtii* flowed within a rectangular tube (*a*) without and (*b*) with phototactic illumination (light source from the right). (*c*,*d*) Schematic of the combined effect of phototaxis and fluid vorticity on the orientation of cells, leading to photo-focusing in the centre (*c*) or on the sides (*d*) of the channel. Adapted from [79]. (Online version in colour.)

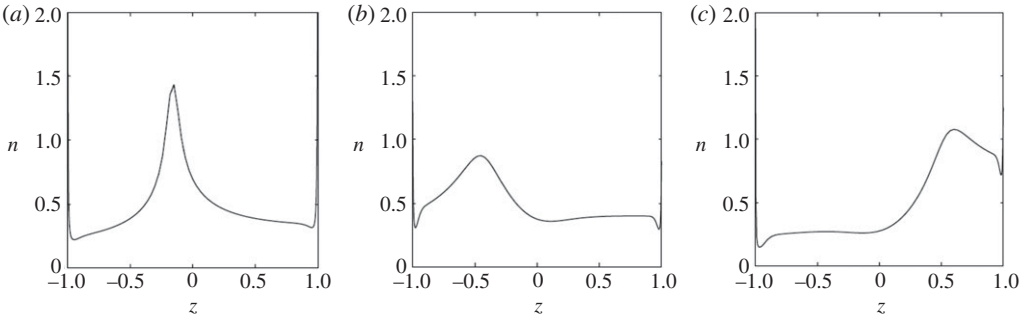

Figure 7. Predicted concentration profiles for phototactic microorganisms within a horizontal Hele–Shaw cell, in the presence of a horizontal background flow and vertical illumination. (*a*) Weak flow ($Pe = 1$), strong absorption and $I_s/I_c = 2$. (*b*) Strong flow ($Pe = 5$), strong absorption and $I_s/I_c = 2$. (*c*) Strong flow ($Pe = 5$), strong absorption and $I_s/I_c = 3$. Adapted from [81].

are not correct, this approach has the advantage that the steady-state concentration profile can be derived analytically.

A systematic theoretical study of photo-focusing of microswimmers in a Poiseuille flow was done by Clarke [81]. He considered a suspension of phototactic cells confined between two no-slip horizontal surfaces located at $z = \pm H/2$ and subjected to a background fluid velocity profile $\boldsymbol{u} = U(1 - 4z^2/H^2)\boldsymbol{e}_x$. Unlike the previous studies, the suspension was uniformly illuminated from below. The local distribution function of cell directions, $f(\boldsymbol{x}, \boldsymbol{p})$, satisfied a generalized form of equation (2.4),

$$(\boldsymbol{u} + \boldsymbol{V}) \cdot \nabla_{\boldsymbol{x}} f + \nabla_{\boldsymbol{p}} \cdot (f\dot{\boldsymbol{p}}) = D_R \nabla_{\boldsymbol{p}}^2 f + D\nabla_{\boldsymbol{x}}^2 f, \tag{5.1}$$

where D is the translational diffusivity and $\boldsymbol{p}$ satisfies equation (2.5) with $1/B = 0$. Phototaxis was implemented through a light dependence of the swimming speed given by model A in

[17] (equation (3.3)), which should be appropriate mostly when the light intensity $I \approx I_c$. The model also considered self-shading within the suspension by modifying the light intensity according to the Beer–Lambert law (equation (3.2)). Within this model, the microorganisms can be concentrated at specific depths within the suspension by adjusting key parameters such as the strength of the flow (defined through the rotational Péclet number $Pe = 2U/(HD_R)$), the cells' absorption coefficient (α in equation (3.2)) and the reduced intensity of the light source I_s/I_c (figure 7). Unfortunately, these studies did not consider the role of bioconvective instabilities due to gravitationally unstable layers induced by photo-focusing in shear flows. We believe that this will provide fertile ground for future investigations.

6. Conclusion

Vigorous bioconvective flows can easily emerge within a suspension of swimming microorganisms and play a fundamental role in nutrient transport, mixing and cell distribution within the suspension. This in turn can have an impact on microbial growth and reproduction, and presents a technological tool to improve the efficiency of bioreactors [84]. We believe that a promising avenue for the rapid and accurate control of bioconvection is to leverage the natural response to light of microbial species. However, the possibility to engineer photo-bioconvection relies on the ability to predict the phototactic behaviour of individual microorganisms. Unfortunately, our understanding of this process is still largely incomplete. Light-induced steering in microalgae has been investigated at both the physiological and biophysical level [34,62,85–87], and much is known about the mechanism of light detection [88], stimulus relay to the flagella [89] and the biomechanics that translates the ensuing changes in flagellar beating into directional changes of the cell [86,90]. Upon illumination, however, cells often switch dynamically between positive and negative taxis, even for a fixed light source. This seemingly unpredictable behaviour is possibly linked to the dual role of light as both an environmental stimulus and energy source, and it highlights the need to investigate in depth the link between cell motility and cell metabolism within a holistic approach to phototaxis. We believe this to be an area prime for substantial developments in the future.

Standard microbial photo-bioconvection is currently restricted to motile eukaryotic microalgae, and although several species are technologically important (e.g. *Dunaliella*, *Chlamydomonas* and *Chlorella* spp. [9]) this still represents a constraint to its general applicability in bioreactors. One possible solution is to engineer a light response within a given species of interest by genetic modification. For example, light regulation of swimming speed, or photokinesis, has recently been introduced in *Escherichia coli*, and used to arrange a bacterial population in complex dynamical patterns of cell concentration in two dimensions [30,31]. In turn, this should be able to generate bioconvection within bulk cultures illuminated from above, providing a first example of genetically engineered photo-bioconvection. Yet another possibility could be offered in the future by light-driven active colloids [91–93]. Currently, they can be made to move microscopic cargo [94,95] and perform phototaxis [91] in two dimensions. If their density is sufficiently reduced, they could swim in bulk towards a light source and drive bioconvective instabilities even in suspensions of non-motile microorganisms.

Overall, the possibilities offered by the combination of phototaxis and bioconvection to control the macroscopic behaviour of active matter suspensions are only starting to be explored. We look forward to the new and exciting developments that will undoubtedly emerge in the future.

Data accessibility. This article has no additional data.

Authors' contributions. All the authors conceived the manuscript; A.J. and M.P. led the writing of the document; J.A. and I.T. helped with manuscript revision.

Competing interests. We declare we have no competing interests.

Funding. A.J., M.P. and I.T. gratefully acknowledge support from The Leverhulme Trust through grant no. RPG-2018-345. J.A. and I.T. acknowledge support from the Spanish Ministry of Economy and Competitiveness

(AEI, FEDER EU) grant nos. FIS2016-77692-C2-1-P and CTM-2017-83774-D. J.A. thanks the Govern de les Illes Balears for financial support through the Vicenç Mut subprogram.

References

1. Platt JR. 1961 'Bioconvection patterns' in cultures of free-swimming organisms. *Science* **133**, 1766–1767. (doi:10.1126/science.133.3466.1766)
2. Bearon RN, Grünbaum D. 2006 Bioconvection in a stratified environment: experiments and theory. *Phys. Fluids* **18**, 127102. (doi:10.1063/1.2402490)
3. Williams CR, Bees MA. 2011 A tale of three taxes: photo-gyro-gravitactic bioconvection. *J. Exp. Biol.* **214**, 2398–408. (doi:10.1242/jeb.051094)
4. Fodor E, Marchetti MC. 2018 The statistical physics of active matter: from self-catalytic colloids to living cells. *Physica A* **504**, 106–120. (doi:10.1016/j.physa.2017.12.137)
5. Wager H. 1911 On the effect of gravity upon the movements and aggregation of *Euglena viridis*, Ehrb., and other micro-organisms. *Phil. Trans. R. Soc. B* **201**, 333–390. (doi:10.1098/rstb.1911.0007)
6. Loefer JB, Mefferd RBJ. 1952 Concerning pattern formation by free-swimming microorganisms. *Am. Nat.* **LXXXVI**, 94–104.
7. Robbins WJ. 1952 Patterns formed by motile *Euglena gracilis* var. *bacillaris*. *Bull. Torrey Botanical Club* **79**, 107. (doi:10.2307/2481929)
8. Plesset MS, Winet H. 1974 Bioconvection patterns in swimming microorganism cultures as an example of Rayleigh–Taylor instability. *Nature* **248**, 7–9. (doi:10.1038/248441a0)
9. Bees MA, Croze OA. 2014 Mathematics for streamlined biofuel production from unicellular algae. *Biofuels* **5**, 53–65. (doi:10.4155/bfs.13.66)
10. Kessler JO, Hill NA. 1997 Complementarity of physics, biology and geometry in the dynamics of swimming micro-organisms. In *Physics of biological systems* (eds H Flyvbjerg, J Hertz, MH Jensen, OG Mouritsen, K Sneppen), pp. 325–340. Berlin, Germany: Springer.
11. Jánosi IM, Czirók A, Silhavy D, Holczinger A. 2002 Is bioconvection enhancing bacterial growth in quiescent environments? *Environ. Microbiol.* **4**, 525–531. (doi:10.1046/j.1462-2920.2002.00328.x)
12. Sommer T *et al.* 2017 Bacteria-induced mixing in natural waters. *Geophys. Res. Lett.* **44**, 9424–9432. (doi:10.1002/2017GL074868)
13. Pedley TJ. 2010 Instability of uniform micro-organism suspensions revisited. *J. Fluid Mech.* **647**, 335. (doi:10.1017/S0022112010000108)
14. Pedley TJ, Kessler JO. 1992 Hydrodynamic phenomena in suspensions of swimming microorganisms. *Annu. Rev. Fluid Mech.* **24**, 313–358. (doi:10.1146/annurev.fl.24.010192.001525)
15. Tuval I, Cisneros L, Dombrowski C, Wolgemuth CW, Kessler JO, Goldstein RE. 2005 Bacterial swimming and oxygen transport near contact lines. *Proc. Natl Acad. Sci. USA* **102**, 2277–2282. (doi:10.1073/pnas.0406724102)
16. Suematsu NJ, Awazu A, Izumi S, Noda S, Nakata S, Nishimori H. 2011 Localized bioconvection of *Euglena* caused by phototaxis in the lateral direction. *J. Phys. Soc. Jpn* **80**, 064003. (doi:10.1143/JPSJ.80.064003)
17. Williams CR, Bees MA. 2011 Photo-gyrotactic bioconvection. *J. Fluid Mech.* **678**, 41–86. (doi:10.1017/jfm.2011.100)
18. Arrieta J, Polin M, Saleta-Piersanti R, Tuval I. 2019 Light control of localized photobioconvection. *Phys. Rev. Lett.* **123**, 158101. (doi:10.1103/PhysRevLett.123.158101)
19. Salek MM, Carrara F, Fernandez V, Guasto JS, Stocker R. 2019 Bacterial chemotaxis in a microfluidic T-maze reveals strong phenotypic heterogeneity in chemotactic sensitivity. *Nat. Commun.* **10**, 1877. (doi:10.1038/s41467-019-09521-2)
20. Sung YJ, Kwak HS, Hong ME, Choi HI, Sim SJ. 2018 Two-dimensional microfluidic system for the simultaneous quantitative analysis of phototactic/chemotactic responses of microalgae. *Anal. Chem.* **90**, 14 029–14 038. (doi:10.1021/acs.analchem.8b04121)
21. Menolascina F, Rusconi R, Fernandez VI, Smriga S, Aminzare Z, Sontag ED, Stocker R. 2017 Logarithmic sensing in *Bacillus subtilis* aerotaxis. *npj Syst. Biol. Appl.* **3**, 16036. (doi:10.1038/npjsba.2016.36)
22. Rusconi R, Garren M, Stocker R. 2014 Microfluidics expanding the frontiers of microbial ecology. *Annu. Rev. Biophys.* **43**, 65–91. (doi:10.1146/annurev-biophys-051013-022916)

23. Lushi E, Goldstein RE, Shelley MJ. 2012 Collective chemotactic dynamics in the presence of self-generated fluid flows. *Phys. Rev. E* **86**, 2–5. (doi:10.1103/PhysRevE.86.040902)
24. Lushi E, Goldstein RE, Shelley MJ. 2018 Nonlinear concentration patterns and bands in autochemotactic suspensions. *Phys. Rev. E* **98**, 052411. (doi:10.1103/PhysRevE.98.052411)
25. Ryan SD. 2019 Role of hydrodynamic interactions in chemotaxis of bacterial populations. *Phys. Biol.* **17**, 016003. (doi:10.1088/1478-3975/ab57af)
26. Ghorai S, Panda M. 2013 Bioconvection in an anisotropic scattering suspension of phototactic algae. *Eur. J. Mech. B. Fluids* **41**, 81–93. (doi:10.1016/j.euromechflu.2012.07.001)
27. Jékely G. 2009 Evolution of phototaxis. *Phil. Trans. R. Soc. B* **364**, 2795–2808. (doi:10.1098/rstb.2009.0072)
28. Razeghifard R. 2013 Algal biofuels. *Photosynth. Res.* **117**, 207–219. (doi:10.1007/s11120-013-9828-z)
29. Ho SH, Nakanishi A, Ye X, Chang JS, Hara K, Hasunuma T, Kondo A. 2014 Optimizing biodiesel production in marine *Chlamydomonas* sp. JSC4 through metabolic profiling and an innovative salinity-gradient strategy. *Biotechnol. Biofuels* **7**, 97. (doi:10.1186/1754-6834-7-97)
30. Arlt J, Martinez VA, Dawson A, Pilizota T, Poon WC. 2019 Dynamics-dependent density distribution in active suspensions. *Nat. Commun.* **10**, 1–7. (doi:10.1038/s41467-019-10283-0)
31. Frangipane G, Dell'Arciprete D, Petracchini S, Maggi C, Saglimbeni F, Bianchi S, Vizsnyiczai G, Bernardini ML, di Leonardo R. 2018 Dynamic density shaping of photokinetic *E. coli*. *eLife* **7**, e36608. (doi:10.7554/eLife.36608)
32. Giometto A, Altermatt F, Maritan A, Stocker R, Rinaldo A. 2015 Generalized receptor law governs phototaxis in the phytoplankton *Euglena gracilis*. *Proc. Natl Acad. Sci. USA* **112**, 7045–7050. (doi:10.1073/pnas.1422922112)
33. Martin M, Barzyk A, Bertin E, Peyla P, Rafai S. 2016 Photofocusing: light and flow of phototactic microswimmer suspension. *Phys. Rev. E* **93**, 1–5. (doi:10.1103/PhysRevE.93.051101)
34. Arrieta J, Barreira A, Chioccioli M, Polin M, Tuval I. 2017 Phototaxis beyond turning: persistent accumulation and response acclimation of the microalga *Chlamydomonas reinhardtii*. *Sci. Rep.* **7**, 3447. (doi:10.1038/s41598-017-03618-8)
35. Bees MA. 2020 Advances in bioconvection. *Annu. Rev. Fluid Mech.* **52**, 449–476. (doi:10.1146/annurev-fluid-010518-040558)
36. Roberts AM. 1970 Geotaxis in motile micro-organisms. *J. Exp. Biol.* **53**, 687–699.
37. Roberts A. 2006 Mechanisms of gravitaxis in *Chlamydomonas*. *Biol. Bull.* **210**, 78–80. (doi:10.2307/4134597)
38. Kage A, Omori T, Kikuchi K, Ishikawa T. 2020 The shape effect of flagella is more important than bottom-heaviness on passive gravitactic orientation in *Chlamydomonas reinhardtii*. *J. Exp. Biol.* **223**, jeb205989. (doi:10.1242/jeb.205989)
39. Kessler JO. 1985 Hydrodynamic focusing of motile algal cells. *Nature* **313**, 218–220. (doi:10.1038/313218a0)
40. Pedley TJ, Hill NA, Kessler JO. 1988 The growth of bioconvection patterns in a uniform suspension of gyrotactic micro-organisms. *J. Fluid Mech.* **195**, 223. (doi:10.1017/S0022112088002393)
41. Pedley TJ, Kessler JO. 1990 A new continuum model for suspensions of gyrotactic micro-organisms. *J. Fluid Mech.* **212**, 155–82. (doi:10.1017/S0022112090001914)
42. Hill NA, Bees MA. 2002 Taylor dispersion of gyrotactic swimming micro-organisms in a linear flow. *Phys. Fluids* **14**, 2598–2605. (doi:10.1063/1.1458003)
43. Hwang Y, Pedley TJ. 2014 Bioconvection under uniform shear: linear stability analysis. *J. Fluid Mech.* **738**, 522–562. (doi:10.1017/jfm.2013.604)
44. Pedley TJ, Kessler JO. 1987 The orientation of spheroidal microoganisms swimming in a flow field. *Proc. R. Soc. Lond. B* **230**, 47–70. (doi:10.1098/rspb.1987.0035)
45. Jeffery G. 1922 The motion of ellipsoidal particles immersed in a viscous fluid. *Proc. R. Soc. Lond. A* **102**, 161. (doi:10.1098/rspa.1922.0078)
46. Kessler JO, Hill NA. 1988 The growth of bioconvection patterns in a uniform suspension of gyrotactic micro-organisms. *J. Fluid Mech.* **195**, 223–237. (doi:10.1017/S0022112088002393)
47. Batchelor GK. 1970 The stress system in a suspension of force-free particles. *J. Fluid Mech.* **41**, 545–570. (doi:10.1017/S0022112070000745)

48. Sharma A, Brader JM. 2016 Communication: Green-Kubo approach to the average swim speed in active Brownian systems. *J. Chem. Phys.* **145**, 161101. (doi:10.1063/1.4966153)
49. Dal Cengio S, Levis D, Pagonabarraga I. 2019 Linear response theory and Green-Kubo relations for active matter. *Phys. Rev. Lett.* **123**, 238003. (doi:10.1103/PhysRevLett.123.238003)
50. Manela A, Frankel I. 2003 Generalized Taylor dispersion in suspensions of gyrotactic swimming micro-organisms. *J. Fluid Mech.* **490**, 99–127. (doi:10.1017/S0022112003005147)
51. Hill NA, Pedley TJ. 2005 Bioconvection. *Fluid Dyn. Res.* **37**, 1–20. (doi:10.1016/j.fluiddyn.2005.03.002)
52. Ghorai S, Hill NA. 2005 Penetrative phototactic bioconvection. *Phys. Fluids* **17**, 074101. (doi:10.1063/1.1947807)
53. Ghorai S, Panda MK, Hill NA. 2010 Bioconvection in a suspension of isotropically scattering phototactic algae. *Phys. Fluids* **22**, 071901. (doi:10.1063/1.3457163)
54. Kessler JO. 1985 Co-operative and concentrative phenomena of swimming micro-organisms. *Contemp. Phys.* **26**, 147–166. (doi:10.1080/00107518508210745)
55. Bees M, Hill N. 1997 Wavelengths of bioconvection patterns. *J. Exp. Biol.* **200**, 1515–1526.
56. Bees MA, Hill NA. 1998 Linear bioconvection in a suspension of randomly swimming, gyrotactic micro-organisms. *Phys. Fluids* **10**, 1864–1881. (doi:10.1063/1.869704)
57. Rafaï S, Jibuti L, Peyla P. 2010 Effective viscosity of microswimmer suspensions. *Phys. Rev. Lett.* **104**, 098102. (doi:10.1103/PhysRevLett.104.098102)
58. Lele PP, Hosu BG, Berg HC. 2013 Dynamics of mechanosensing in the bacterial flagellar motor. *Proc. Natl Acad. Sci. USA* **110**, 11 839–11 844. (doi:10.1073/pnas.1305885110)
59. Ghorai S, Hill NA. 2007 Gyrotactic bioconvection in three dimensions. *Phys. Fluids* **19**, 054107. (doi:10.1063/1.2731793)
60. Karimi A, Paul MR. 2013 Bioconvection in spatially extended domains. *Phys. Rev. E* **87**, 053016. (doi:10.1103/PhysRevE.87.053016)
61. Ghorai S, Singh R, Hill NA. 2015 Wavelength selection in gyrotactic bioconvection. *Bull. Math. Biol.* **77**, 1166–1184. (doi:10.1007/s11538-015-0081-9)
62. Foster KW, Smyth RD. 1980 Light antennas in phototactic algae. *Microbiol. Rev.* **44**, 572–630. (doi:10.1128/MMBR.44.4.572-630.1980)
63. Moldrup M, Garm A. 2012 Spectral sensitivity of phototaxis in the dinoflagellate *Kryptoperidinium foliaceum* and their reaction to physical encounters. *J. Exp. Biol.* **215**, 2342–2346. (doi:10.1242/jeb.066886)
64. Crescitelli F, James T, Erickson J, Loew E, McFarland W. 1992 The eyespot of *Chlamydomonas reinhardtii*: a comparative microspectrophotometric study. *Vision Res.* **32**, 1593–1600. (doi:10.1016/0042-6989(92)90152-9) GB.
65. Harris EH, Stern DB, Witman GB. 2009 *The Chlamydomonas sourcebook*, vol. 2. New York, NY: Academic Press.
66. Yamamoto Y, Okayama T, Sato K, Takaoki T. 1992 Relation of pattern formation to external conditions in the flagellate, *Chlamydomonas reinhardtii*. *Eur. J. Protistol* **28**, 415–420. (doi:10.1016/S0932-4739(11)80005-2)
67. Vincent RV, Hill NA. 1996 Bioconvection in a suspension of phototactic algae. *J. Fluid Mech.* **327**, 343–371. (doi:10.1017/S0022112096008579)
68. Panda MK, Singh R, Mishra AC, Mohanty SK. 2016 Effects of both diffuse and collimated incident radiation on phototactic bioconvection. *Phys. Fluids* **28**, 124104. (doi:10.1063/1.4972057)
69. Panda MK, Ghorai S. 2013 Penetrative phototactic bioconvection in an isotropic scattering suspension. *Phys. Fluids* **25**, 071902. (doi:10.1063/1.4813402)
70. Yang Y *et al.* 2018 Phototaxis in a wild isolate of the cyanobacterium *Synechococcus elongatus*. *Proc. Natl Acad. Sci. USA* **115**, E12378–E12387. (doi:10.1073/pnas.1812871115)
71. Sengupta A, Carrara F, Stocker R. 2017 Phytoplankton can actively diversify their migration strategy in response to turbulent cues. *Nature* **543**, 555–558. (doi:10.1038/nature21415)
72. Bearon RN, Hazel AL, Thorn GJ. 2011 The spatial distribution of gyrotactic swimming micro-organisms in laminar flow fields. *J. Fluid Mech.* **680**, 602–635. (doi:10.1017/jfm.2011.198)
73. Bearon RN, Bees MA, Croze OA. 2012 Biased swimming cells do not disperse in pipes as tracers: a population model based on microscale behaviour. *Phys. Fluids* **24**, 121902. (doi:10.1063/1.4772189)

74. Bearon RN, Hazel AL. 2015 The trapping in high-shear regions of slender bacteria undergoing chemotaxis in a channel. *J. Fluid Mech.* **771**, R3. (doi:10.1017/jfm.2015.198)
75. Suematsu NJ. 2014 Localized ordered pattern in a hybrid system of hydrodynamics and collective motion. *JPSJ News Comments* **11**, 06. (doi:10.7566/JPSJNC.11.06)
76. Shoji E, Nishimori H, Awazu A, Izumi S, Iima M. 2014 Localized bioconvection patterns and their initial state dependency in *Euglena gracilis* suspensions in an annular container. *J. Phys. Soc. Jpn* **83**, 043001. (doi:10.7566/JPSJ.83.043001)
77. Dervaux J, Capellazzi Resta M, Brunet P. 2017 Light-controlled flows in active fluids. *Nat. Phys.* **13**, 306–312. (doi:10.1038/nphys3926)
78. Furlan S, Comparini D, Ciszak M, Beccai L, Mancuso S, Mazzolai B. 2012 Origin of polar order in dense suspensions of phototactic micro-swimmers. *PLoS ONE* **7**, e38895. (doi:10.1371/journal.pone.0038895)
79. Garcia X, Rafaï S, Peyla P. 2013 Light control of the flow of phototactic microswimmer suspensions. *Phys. Rev. Lett.* **110**, 138106. (doi:10.1103/PhysRevLett.110.138106)
80. Jibuti L, Qi L, Misbah C, Zimmermann W, Rafaï S, Peyla P. 2014 Self-focusing and jet instability of a microswimmer suspension. *Phys. Rev. E* **90**, 063019. (doi:10.1103/PhysRevE.90.063019)
81. Clarke RJ. 2018 Photofocusing of microorganisms swimming in a flow with shear. *ANZIAM J.* **59**, 455–471. (doi:10.21914/anziamj.v59i0.12272)
82. Zöttl A, Stark H. 2012 Nonlinear dynamics of a microswimmer in Poiseuille flow. *Phys. Rev. Lett.* **108**, 218104. (doi:10.1103/PhysRevLett.108.218104)
83. Croze OA, Bearon RN, Bees MA. 2017 Gyrotactic swimmer dispersion in pipe flow: testing the theory. *J. Fluid Mech.* **816**, 481–506. (doi:10.1017/jfm.2017.90)
84. Bees MA, Croze OA. 2010 Dispersion of biased swimming micro-organisms in a fluid flowing through a tube. *Proc. R. Soc. A* **466**, 2057–2077. (doi:10.1098/rspa.2009.0606)
85. Drescher K, Goldstein RE, Tuval I. 2010 Fidelity of adaptive phototaxis. *Proc. Natl Acad. Sci. USA* **107**, 11 171–11 176. (doi:10.1073/pnas.1000901107)
86. Leptos KC, Chioccioli M, Furlan S, Pesci AI, Goldstein RE. 2018 An adaptive flagellar photoresponse determines the dynamics of accurate phototactic steering in *Chlamydomonas*. (https://www.biorxiv.org/content/10.1101/254714v2)
87. de Maleprade H, Moisy F, Ishikawa T, Goldstein RE. 2019 Motility and phototaxis of *Gonium*, the simplest differentiated colonial alga. *Phys. Rev. E* **101**, 022416. (doi:10.1101/845891)
88. Kateriya S, Nagel G, Bamberg E, Hegemann P. 2004 'Vision' in single-celled algae. *Physiology* **19**, 133–137. (doi:10.1152/nips.01517.2004)
89. Govorunova EG, Sineshchekov OA, Hegemann P. 1997 Desensitization and dark recovery of the photoreceptor current in *Chlamydomonas reinhardtii*. *Plant Physiol.* **115**, 633–642. (doi:10.1104/pp.115.2.633)
90. Josef K, Saranak J, Foster KW. 2006 Linear systems analysis of the ciliary steering behavior associated with negative-phototaxis in *Chlamydomonas reinhardtii*. *Cell Motil. Cytoskeleton* **63**, 758–77. (doi:10.1002/cm.20158)
91. Lozano C, Löwen H, Bechinger C. 2016 Phototaxis of synthetic microswimmers in optical landscapes. *Nat. Commun.* **7**, 12828. (doi:10.1038/ncomms12828)
92. Gomez-Solano JR, Samin S, Lozano C, Ruedas-Batuecas P, van Roij R, Bechinger C. 2017 Tuning the motility and directionality of self-propelled colloids. *Sci. Rep.* **7**, 14891. (doi:10.1038/s41598-017-14126-0)
93. Maggi C, Angelani L, Frangipane G, Di Leonardo R. 2018 Currents and flux-inversion in photokinetic active particles. *Soft Matter* **14**, 4958–4962. (doi:10.1039/C8SM00788H)
94. Ibele M, Mallouk TE, Sen A. 2009 Schooling behavior of light-powered autonomous micromotors in water. *Angew. Chem. Int. Ed.* **48**, 3308–3312. (doi:10.1002/anie.200804704)
95. Hong Y, Diaz M, Córdova-Fteueroa UM, Sen A. 2010 Light-driven titanium-dioxide-based reversible microfireworks and micromotor/micropump systems. *Adv. Funct. Mater.* **20**, 1568–1576. (doi:10.1002/adfm.201000063)